JACS
JOURNAL OF THE AMERICAN CHEMICAL SOCIETY
Article
Cite This: J. Am. Chem. Soc. 2018, 140, 12256−12262
pubs.acs.org/JACS

$PdSeO_3$ Monolayer: Promising Inorganic 2D Photocatalyst for Direct Overall Water Splitting Without Using Sacrificial Reagents and Cocatalysts

Man Qiao,[†] Jie Liu,[†] Yu Wang,[†] Yafei Li,*[,†] and Zhongfang Chen*[,‡]

[†]Jiangsu Collaborative Innovation Centre of Biomedical Functional Materials, School of Chemistry and Materials Science, Nanjing Normal University, Nanjing 210023, China

[‡]Department of Chemistry, University of Puerto Rico, Rio Piedras Campus, San Juan, PR 00931, United States

Supporting Information

ABSTRACT: Direct production of H_2 from photocatalytic water splitting is a potential solution to environmental pollution and energy crisis, and tremendous efforts have been made to seek efficient photocatalysts that can split pure water (pH = 7) under visible light irradiation. Herein, by means of systematic density functional theory (DFT) computations, we demonstrated that the two-dimensional (2D) $PdSeO_3$ monolayer is a promising candidate. The mechanical exfoliation of $PdSeO_3$ monolayer from its bulk phase is experimentally feasible due to the relatively small cleavage energy of ~0.42 J/m^2. Remarkably, $PdSeO_3$ monolayer is semiconducting with a moderate indirect band gap of 2.44 eV, and its valence and conduction bands perfectly engulf the redox potentials of water. In particular, water oxidation and hydrogen reduction half reactions can both occur readily on the different active sites of $PdSeO_3$ monolayer under the potentials solely provided by photogenerated electrons and holes. As $PdSeO_3$ monolayer also has rather pronounced optical absorption in the visible and ultraviolet regions of the solar spectrum, it could be utilized as a highly efficient photocatalyst for splitting pure water into H_2 and O_2 in a stoichiometric amount of 2:1 without using sacrificial reagents or cocatalysts.

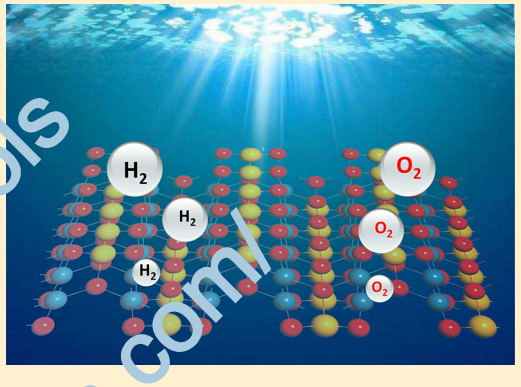

INTRODUCTION

Since the pioneering work by Fujishima and Honda et al.,[1] utilizing sunlight irradiation to split water into hydrogen (H_2) and oxygen (O_2) with the help of photocatalysts has become a promising way to convert solar energy into chemical energy.[2−7] In principle, an efficient photocatalyst for water splitting must satisfy several criteria. First, the bandgap of photocatalyst must exceed the free energy (ΔG) of water splitting (1.23 eV) but be lower than 3.0 eV in order to efficiently utilize the solar energy.[7,8] Second, the photogenerated carriers should be transferred rapidly and separated efficiently to avoid the surface charge recombination. More importantly, the photocatalyst should have a suitable band edge alignment, namely, the conduction band minimum (CBM) must be higher than the reduction potential of H^+/H_2 (−4.44 eV at pH = 0) and the valence band maximum (VBM) must be lower than the oxidation potential of O_2/H_2O (−5.67 eV at pH = 0).[9,10] In the past decades, many three-dimensional (3D) bulk materials, including but not limited to transition metal oxides,[11−13] oxysulfides,[14,15] and oxynitrides[16,17] have been identified as promising photocatalysts for water splitting. However, most 3D photocatalysts cannot trigger water redox reactions on the surfaces due to the absence of active sites; consequently, the cocatalysts (e.g., Pt, Ni, IrO_2) should be loaded to facilitate reactions by providing the active sites and suppressing the charge recombination.[18]

Since the experimental realization of graphene by Geim et al. in 2004,[19] two-dimensional (2D) materials have been a subject of extensive experimental and theoretical studies due to its many excellent electronic, optical, and mechanical properties.[20−23] Compared to their 3D bulk counterparts, 2D structures can provide ultrahigh surface area for photochemical reactions and minimum migration distance for carriers, which are desirable for achieving highly efficient photocatalysis. Therefore, 2D semiconducting materials with a band gap in the range of 1.5−3.0 eV have been intensively investigated in recent years as they are ideal candidates for fabricating water splitting photocatalysts.[24−33] Unfortunately, though some 2D structures have suitable band edges that absolutely straddle the redox potentials of water, the photogenerated electrons and holes may not process sufficient driving force for overall water splitting. Note that the hydrogen reduction half reaction involves a two-electron transfer process, whereas water oxidation half reaction involves a more complicated four-electron transfer process, thus a considerable overpoential is

Received: July 24, 2018
Published: August 31, 2018

Downloaded via UNIV OF PUERTO RICO AT RIO PIEDRAS on July 27, 2019 at 03:34:23 (UTC).
See https://pubs.acs.org/sharingguidelines for options on how to legitimately share published articles.

Solid PDF Tools
http://www.SolidDocuments.com/

© 2018 American Chemical Society

DOI: 10.1021/jacs.8b07855
J. Am. Chem. Soc. 2018, 140, 12256−12262

usually required to ensure that the two reactions can spontaneously proceed. For example, the most investigated 2D water-splitting photocatalyst g-C_3N_4[34,35] and the recently unveiled 2D MPS_3 (M = Ni, Mn, and Fe)[36−38] can show rather good photocatalytic activity for H_2 evolution, but they all suffer from the large overpotential of water oxidation half reaction. Generally, the water oxidation half reaction can be suppressed by adding sacrificial reagents, but it is rather undesirable for practical applications.[39] At present, most experimentally investigated 2D photocatalysts require the loading of catalysts (e.g., CoOx)[40] to realize overall water-splitting. Therefore, seeking efficient 2D photocatalysts that can directly split pure water without using sacrificial reagents and cocatalysts is of great importance and remains a big challenge.

Experimentally, many 2D structures (e.g., MoS_2,[41] *h*-BN,[42] and black phosphorene[43]) have been realized via mechanical or liquid exfoliation from their bulk counterparts, which provides us a feasible way to explore more 2D photocatalyst for water splitting. For example, Jing et al. recently proposed that palladium phosphide sulfide (PdPS) monolayer,[44] which can be easily exfoliated from the PdPS bulk, is a stable 2D structure with suitable electronic and optical properties for photocatalytic water splitting. In 2007, Ling et al. synthesized a novel Pd compound, namely $PdSeO_3$,[45] in which all the Pd atoms have a square-planar coordination. Similar to PdPS, $PdSeO_3$ is also a layered material with interlayer van der Waals (vdW) bonding. Thus, it is highly possible to achieve single-layered $PdSeO_3$ by exfoliating the corresponding bulk. However, to date $PdSeO_3$ monolayer has not been synthesized, and the electronic and optical properties of $PdSeO_3$ monolayer are yet to be explored.

In this work, we systematically investigated the structural, electronic, and optical properties of $PdSeO_3$ monolayer by means of comprehensive density functional theory (DFT) computations. It is found that $PdSeO_3$ monolayer is thermodynamically and kinetically stable and can be obtained via exfoliation strategies. Remarkably, $PdSeO_3$ monolayer has a moderate band gap (2.84 eV), presents suitable band edge alignments, and can provide adequate driving force for water splitting. As $PdSeO_3$ monolayer also has pronounced absorption in the visible region of the solar spectrum, it could be a highly promising photocatalyst for direct overall water splitting.

COMPUTATIONAL METHODS

All the DFT calculations were performed using the Vienna ab initio simulation package (VASP).[46] The electron−ion interaction was described using the projector augmented wave (PAW) approach.[47,48] The exchange-correlation term was described by the Perdew−Burke−Ernzerhof (PBE) functional[49] within the generalized gradient approximation (GGA) except that the HSE06 hybrid functional[50] with a mixing parameter alpha value of 0.25 was utilized to evaluate the electronic properties. The spin−orbital coupling (SOC) effect was also taken into account in band structure computations. We used the DFT-D3 (D stands for dispersion) procedure to account for van der Waals (vdW) interactions.[51] A 550 eV cutoff for the plane wave expansion was adopted in all the computations.

Geometries were optimized until the convergence criteria of energy and force were less than 10^{-5} eV and 0.02 eV/Å, respectively. A Monkhorst−Pack *k*-point mesh of 15 × 9 × 1 and 19 × 11 × 1 was used to sample the 2D Brillouin zone for geometry optimizations and electronic structure computations, respectively. We set the *x* and *y* directions parallel and the *z* direction perpendicular to the layer plane and adopted a supercell length of 40 Å in the *z* direction. The phonon band structure of $PdSeO_3$ monolayer was computed using the density functional perturbation theory (DFPT)[52] as implemented in the PHONOPY package.[53] We used a large 3 × 7 × 1 supercell with a *k*-mesh of 5 × 5 × 1 for Brillouin zone integrations and a cutoff energy of 550 eV for the plane-wave basis set. The first-principles molecular dynamics (FPMD) simulations were carried out to assess the thermal stability of the $PdSeO_3$ monolayer. At each temperature, the FPMD simulation in NVT ensemble last for 10 ps with a time step of 1.0 fs. The temperature was controlled by using the Nosé−Hoover method.[54] The solvation effects in aqueous solution were considered with the Poisson−Boltzmann implicit solvation model, where the dielectric constant of water was taken as 80.[55]

To compute the free energy change (ΔG) in the hydrogen reduction and water oxidation reactions, we adopted the method developed by Nørskov et al.,[56,57] according to which the ΔG of an electrochemical reaction is computed as

$$\Delta G = \Delta E + \Delta E_{zpe} - T\Delta S + \Delta G_{pH} + \Delta G_U$$

where ΔE is the DFT computed reaction (electronic) energy, ΔE_{ZPE} and ΔS are the zero-point energy difference and the entropy difference between the adsorbed state and the gas phase, respectively, and T is the system temperature (298.15 K, in our work). For each system, its E_{zpe} can be calculated by summing vibrational frequencies over all normal modes ν ($E_{zpe} = 1/2\Sigma h\nu$). The entropies of the free molecules (O_2, H_2, and H_2O) were taken from the NIST database.[58] $\Delta G_{pH} = 0.059 \times pH$ represents the free-energy contribution due to the variation in H concentration. We considered the effect of a potential bias on all states involving one electron or hole in the electrode by shifting the energy of this energy by $\Delta G_U = -eU$, where U is the electrode potential relative to the standhard hydrogen electrode (SHE). For those reactions involving the release of protons and electrons, the free energy of one pair of proton and electron ($H^+ + e^-$) at standard conditions ($pH = 0$, $U = 0$) was taken as $1/2G_{H2}$. The free energy of O_2(g) was derived as $G_{O2} = 2G_{H2O} - 2G_{H2} - 4.92$ eV since O_2 in triplet ground state is notoriously poorly described by DFT calculations.

RESULTS AND DISCUSSION

Geometric Structure and Stability of $PdSeO_3$ Monolayer. Bulk $PdSeO_3$ is a natural layered material which crystallizes in a monoclinic structure with the space group $P2_1/m$ (No. 11). As shown in Figure 1a, $PdSeO_3$ layers are stacked together with interlayer vdW bonding along the *z* axis. The equilibrium lattice parameters of $PdSeO_3$ bulk were optimized to be *a* = 3.94 Å, *b* = 6.49 Å, *c* = 6.10 Å, and β = 96.20° at the

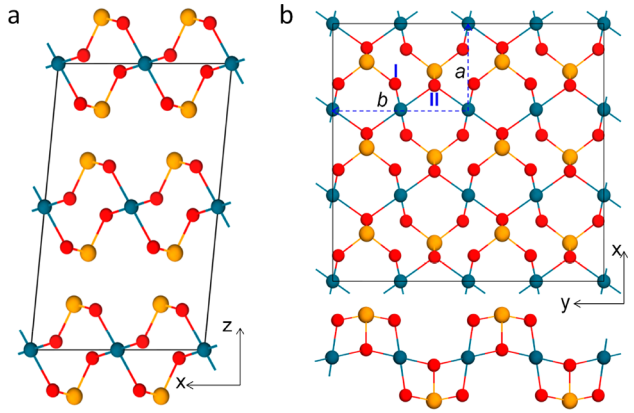

Figure 1. (a) Crystal structure of $PdSeO_3$ bulk. (b) Top and side views of the optimized structure of $PdSeO_3$ monolayer with two basic vectors *a* and *b*. The blue, brown, and red balls represent Pd, Se, and O atoms, respectively. The dashed rectangle marks the primitive cell of the monolayer. The 2-coordinate and 3-coordinate O atoms are denoted by I and II labels, respectively.

http://www.SolidDocuments.com/ Solid PDF Tools

DOI: 10.1021/jacs.8b07855
J. Am. Chem. Soc. 2018, 140, 12256−12262

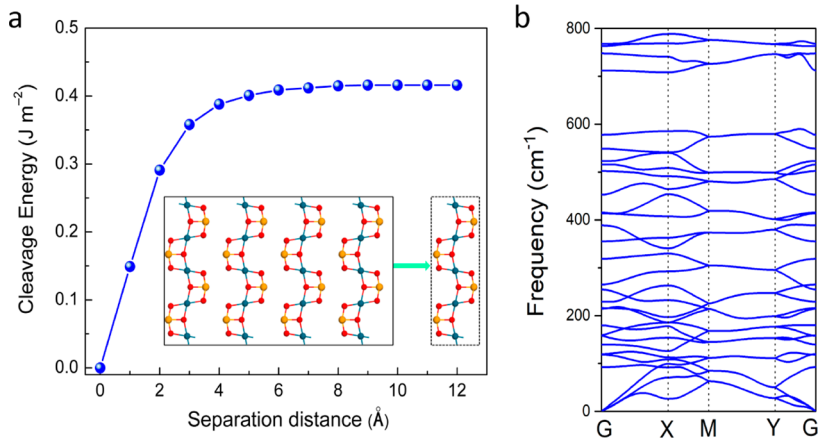

Figure 2. (a) Cleavage energy as a function of the separation distance for a fracture in bulk $PdSeO_3$. The inset is the schematic of separating a monolayer from its neighboring four-layer. The distance of zero refers to the equilibrium geometry. (b) Phonon dispersion curves of the $PdSeO_3$ monolayer.

PBE-D3 level of theory, which are in good agreement with the experimentally measured values (a = 3.89 Å, b = 6.42 Å, c = 6.11 Å, and β = 96.21°).[45]

In one individual $PdSeO_3$ layer, each Pd atom is uniformly bound to four O atoms in the same plan to form a square planar geometry (PdO_4). Actually, the square planar coordination is quite common for Pd^{2+} and has been observed in many Pd-containing layered compounds (e.g., $PdSe_2$,[59] PdPS,[44] and Pd_2Se_3[60]). Each Se atom also uniformly binds with three O atoms to form a trigonal pyramidal selenite anion (SeO_3^{2-}). In contrast to Pd and Se, O atoms of $PdSeO_3$ can be divided into O_I and O_{II} subgroups according to the different bonding patterns, which are two-coordinate and three-coordinate, respectively. Generally, in the $PdSeO_3$ layer, PdO_4 units are connected together through corner sharing to form zigzag chains along the y axis, which are further lined by SeO_3^{2-} anions along the x axis to form layered structure. The structure of $PdSeO_3$ monolayer can be easily obtained by isolating an individual layer from the $PdSeO_3$ bulk. The optimized lattice parameters of $PdSeO_3$ monolayer (a = 3.99 Å and b = 6.49 Å) are slightly larger than those of the bulk phase. Detailed structural properties of bulk and monolayer $PdSeO_3$ are summarized in Table S1.

Experimentally, many 2D structures can be produced from their layered bulk materials via mechanical or liquid exfoliation,[41−43] while the latter is more suitable for those with relatively strong interlayer interaction. After examining the structural properties of $PdSeO_3$ monolayer, we evaluated the feasibility to obtain this 2D structure via the exfoliation techniques by computing the cleavage energy (E_{cl}) of $PdSeO_3$ monolayer. In this work, the cleavage energy was determined by imposing a fracture in a five-layer slab model of $PdSeO_3$, in which the top layer is removed while the rest, the four layers, are fixed. The total energy under variation of the separation distance (d) between two components was then computed to simulate the exfoliation process. As shown in Figure 2a, the E_{cl} of $PdSeO_3$ monolayer first increases rapidly with increasing separation distance and then gradually converges to a constant value of ~0.42 J/m^2 when the separation distance is larger than 4 Å. Remarkably, the E_{cl} of $PdSeO_3$ monolayer is quite close to that of graphene (0.37 J/m^2),[61] indicative of a weak interlayer interaction in $PdSeO_3$ and a high feasibility of obtaining $PdSeO_3$ monolayer via mechanical exfoliation.

The kinetic stability of the $PdSeO_3$ monolayer was confirmed by the phonon curves shown in Figure 2b, where no appreciable imaginary phonon mode can be observed. Especially, the highest frequency of $PdSeO_3$ monolayer reaches up to 760 cm^{-1}, which is higher than those of MoS_2 monolayer (471 cm^{-1})[62] and silicene (550 cm^{-1}),[63] indicative of the robust chemical bonds in $PdSeO_3$ monolayer.

Moreover, we also performed FPMD simulations to assess the thermal stability of $PdSeO_3$ monolayer. Considering the confinement of periodic boundary conditions, a relatively large 4 × 3 supercell consisting of 120 atoms was adopted in the simulations. The FPMD simulations at temperatures of 500, 1000, and 1500 K demonstrate that the structure of $PdSeO_3$ monolayer can be well kept throughout a 10 ps simulation up to 1000 K (Figure S1). In addition, we carried out geometry optimization starting from the distorted structure by FPMD at 1000 K and found that it can be easily relaxed to the initial configuration. The simulations manifest that $PdSeO_3$ monolayer has rather good thermal stability as it can be separated by an adequate barrier from other minimum structures on the potential energy surface.

Electronic Properties of $PdSeO_3$ Monolayer. Having identified the experimental feasibility and intrinsic stability of the $PdSeO_3$ monolayer, we then investigated its electronic properties by computing the band structure and density of states (DOS). $PdSeO_3$ monolayer is semiconducting with an indirect band gap of 2.84 eV computed at the HSE06+SOC level of theory (Figure 3). The valence band maximum (VBM) is located at the X (0.5, 0, 0) point, whereas the conduction band minimum (CBM) lies at the Γ (0, 0, 0) point. The direct band gap at the Γ point (3.07 eV) is quite close to the indirect band gap. According to the analysis of partial DOS, both VBM and CBM of $PdSeO_3$ monolayer are contributed mainly by Pd 4d states and partially by O 2p states, whereas the contribution of Se 4p states to both VBM and CBM is insignificant.

As stated before, semiconducting materials with a band gap in the range of 1.23−3.00 eV may have applications in photocatalytic water splitting. To assess the possibility of using $PdSeO_3$ monolayer as a photocatalyst for water splitting, we further aligned its band edge positions with vacuum level corrections and compared with the potentials of hydrogen reduction (−4.44 eV) and water oxidation (−5.67 eV) reactions. As shown in Figure 3, at pH = 0 the CBM position

Solid PDF Tools
http://www.SolidDocuments.com/

DOI: 10.1021/jacs.8b07855
J. Am. Chem. Soc. 2018, 140, 12256−12262

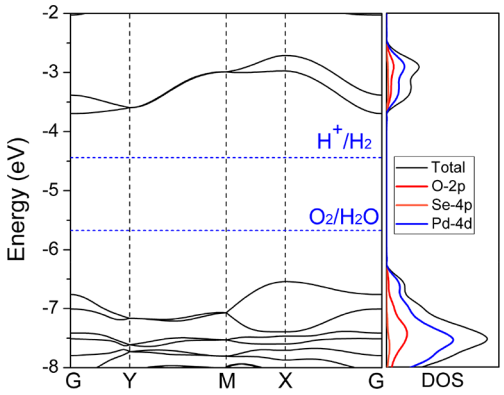

Figure 3. Band structure (left) and density of states (DOS) (right) of $PdSeO_3$ monolayer. The energy level positions have been corrected by vacuum level. The water redox potentials at pH = 0 are marked by the blue dotted lines.

of $PdSeO_3$ monolayer (−3.70 eV) is higher than the hydrogen reduction potential while the VBM position of (−6.54 eV) is lower than the water oxidation potential, fulfilling the thermodynamic requirements for overall water splitting. Encouragingly, the electronic properties of $PdSeO_3$ are less dependent on the thickness due to the rather weak interlayer interaction, and the band edge positions of $PdSeO_3$ bilayer and trilayer are also suitable for photocatalytic water splitting at pH = 0 (Figure S2). As the pH dependence of band positions relative to the SHE is on the exactly same order as the pH dependence of water redox potentials (0.059 × pH),[64] $PdSeO_3$ nanosheet in principle is capable of catalyzing water splitting at all pH values (Figure S3). In what follows we mainly focused on $PdSeO_3$ monolayer as it has the highest ratio of surface atoms.

For photocatalytic water splitting, the magnitude of external potentials provided by photogenerated carriers directly determines whether the water splitting half reactions can proceed spontaneously. The potential of photogenerated electrons for hydrogen reduction reaction (U_e), which is defined as the energy difference between the hydrogen reduction potential and the CBM, was found to be 0.74 V for $PdSeO_3$ monolayer at pH = 0. The potential of photogenerated holes for water oxidation (U_h), which is defined as the energy difference between the VBM and the hydrogen reduction potential, was determined to be 2.10 V at pH = 0. As U_e and U_h are treated as the electrode potential relative to the SHE, they change with the pH according to U_e = 0.74 + 0.059 × pH and U_h = 2.10−0.059 × pH, respectively. Therefore, at pH = 7 the U_e and U_h should be 1.15 and 1.69 V, respectively, which indicates the good photocatalytic activity of $PdSeO_3$ monolayer in the neutral environment. Moreover, the high U_e and U_h also manifest that the photogenerated electrons and holes of $PdSeO_3$ monolayer would prefer to be transferred

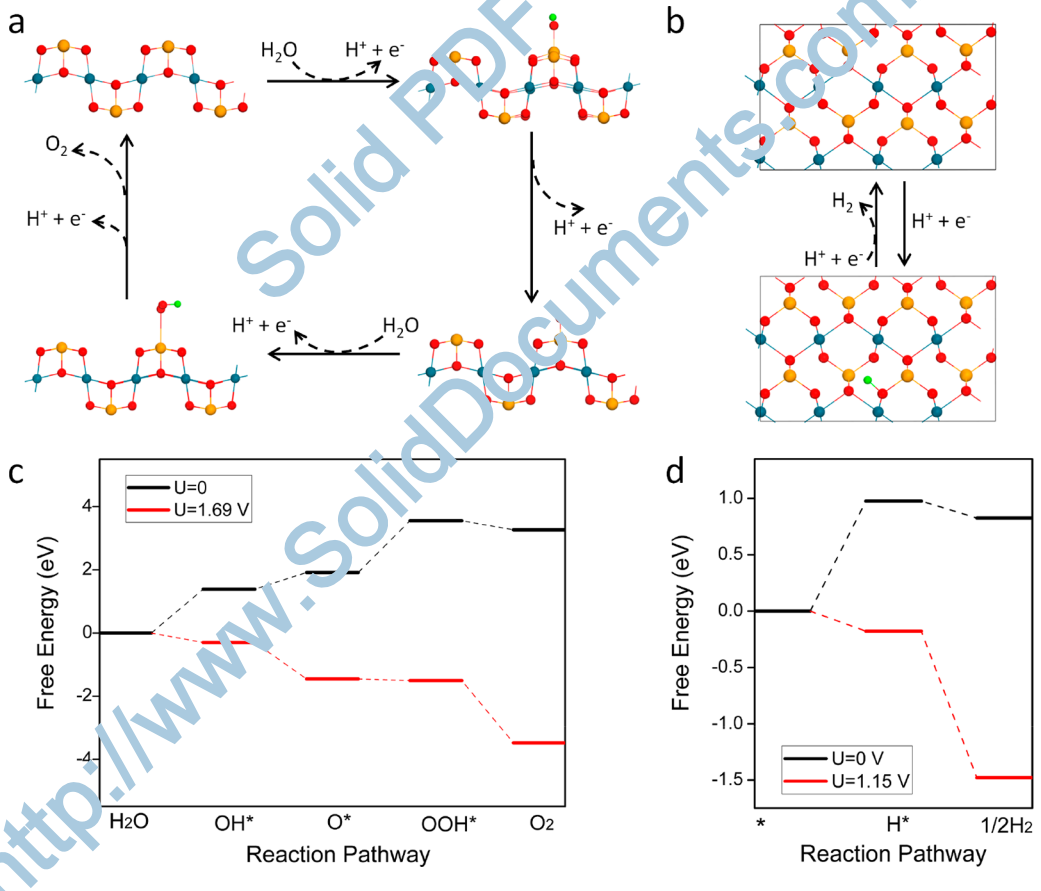

Figure 4. Proposed photocatalytic pathways of (a) water oxidation and (b) hydrogen reduction half reactions with the most energetically favorable absorbed intermediates (OH*, O*, OOH*, and H*) in $PdSeO_3$ monolayer. The red and green balls represent O and H atoms, respectively. Free-energy diagrams for the 4e pathways of water oxidation and 2e pathways of hydrogen reduction reactions in $PdSeO_3$ monolayer. U = 1.69 V and U = 1.15 V are potentials provided by photogenerated holes and electrons for water oxidation and hydrogen reduction reactions at pH = 7, respectively.

Solid PDF Tools
http://www.SolidDocuments.com/

DOI: 10.1021/jacs.8b07855
J. Am. Chem. Soc. 2018, 140, 12256−12262

to react with water rather than with itself, resulting in a good resistance to the photoinduced corrosion.[65]

Overall Water Splitting on $PdSeO_3$ Monolayer. The availability of suitable band edge positions does not guarantee that the $PdSeO_3$ monolayer will be an efficient photocatalyst for overall water splitting, since we are not sure whether the photogenerated electrons and holes of $PdSeO_3$ monolayer can provide an adequate driving force to trigger the overall water splitting. To this end, we systematically investigated mechanisms of both water oxidation and hydrogen reduction half reactions to gain deeper insights into the photocatalytic activity of $PdSeO_3$ monolayer. As it is preferable that the water splitting can occur in the neutral environment, the pH value was set to be 7 in the following studies.

We first studied the more complicated water oxidation half reaction on the surface of $PdSeO_3$ monolayer following the four-electron (4e) reaction pathway, which is accompanied by the formation of adsorbed OH*, O*, and OOH* intermediates. The free energies of water oxidation intermediates (Table S2) and the reaction free energies (ΔG) of elementary steps at pH = 7 were then computed. Figure 4a presents the atomic configurations of intermediates along the reaction pathway of water oxidation on the $PdSeO_3$ monolayer, and the corresponding free-energy profiles are summarized in Figure 4c. We initially considered the situation without any external potential to simulate the condition in the absence of any light irradiation (U_h = 0). For the first step of water oxidation, the water molecule is transferred to a *OH species, which favors to be adsorbed on the top of Se site with a ΔG of 1.39 eV. Next, the *OH species can be oxidized to be the O* species by releasing an electron and a proton. This step is also endothermic by 0.53 eV in the free-energy profile. In the third step, the O* species reacts with another water molecule to form an OOH* species with a ΔG of 1.63 V, which is higher than those of the first two steps. Finally, the *OOH species can release one electron–proton pair to form a spontaneously released O_2 molecule. Interestingly, this step is exothermic by 0.29 eV at pH = 7. Note that it is very important to include solvation effect as performed above to well describe the thermodynamics of chemical reactions that occur at the solid/liquid interfaces; for example, as compared with the gas phase data, the adsorption energies of OH* and OOH* species are ~0.15 eV stronger when taking account the solvation effect. The above results indicate that the water oxidation half reaction is energetically rather unfavorable on the surface of $PdSeO_3$ monolayer in the absence of light irradiation, and the rate-limiting step is the conversion of O* to OOH* with a limiting potential (U_{lim}) of −1.63 V. Therefore, $PdSeO_3$ monolayer requires a relatively small external potential of 1.63 V to drive the whole reaction at pH = 7, which is much lower than that of g-C_3N_4 (2.28 V).[66] On the basis of the simple relationship between limiting potential (U_{lim}) and overpotential (η), $\eta = -0.82\ V - U_{lim}$, where −0.82 V (−1.23 + 0.059 × 7 = −0.82 V) is the equilibrium potential of water oxidation at pH = 7; we can evaluate that the water oxidation overpotential of $PdSeO_3$ monolayer is 0.81 V.

Encouragingly, after shifting the energy of these charge-involved steps by $-eU$ (U_h = 1.69 V) to take account of the external potential provided by photogenerated holes, all the four elementary steps become downhill in the free-energy profile (Figure 4c), indicating that $PeSeO_3$ monolayer is capable of catalyzing water oxidation in the neutral environment under light irradiation. In sharp contrast, though the photogenerated holes of g-C_3N_4 can provide a larger external potential (U_h = 1.85 V) than that of $PdSeO_3$ monolayer at pH = 7, the water oxidation half reaction is essentially prevented to proceed spontaneously on g-C_3N_4 due to the large overpotential (1.56 V).[67] Therefore, $PeSeO_3$ monolayer should have a higher activity than g-C_3N_4 toward water oxidation. Moreover, beside Se sites, we also considered other sites of $PeSeO_3$ monolayer (Table S3) but found that they are actually inert for water oxidation.

In contrast to water oxidation, the active sites for hydrogen reduction half reaction are the O_I sites rather than the Se sites (Table S3). The different active sites for two half reactions would significantly facilitate the high efficient photocatalysis. In the absence of light irradiation (U = 0), $PdSeO_3$ monolayer exhibits an energetically unfavorable ΔG of 0.98 eV for the formation of H* species, while the formation of H_2 molecule from H* species is exothermic by 0.15 eV at pH = 7 (Figure 4d). Remarkably, under the external potential provided by photogenerated electrons (U_e = 1.15 V), the two elementary steps of hydrogen reduction reaction are both downhill in the free-energy profile. Therefore, our results vividly show that $PdSeO_3$ monolayer is able to efficiently split pure water under light irradiation as both water oxidation and hydrogen reduction half reactions can proceed spontaneously. To the best of our knowledge, $PdSeO_3$ monolayer is the first ever reported inorganic 2D material than can act as a highly efficient photocatalyst for direct overall water splitting without using any cocatalysts.

Optical Properties of $PdSeO_3$ Monolayer. An efficient photocatalyst should have a strong power to harvest solar light, especially the ultraviolet and visible light. To give an intuitive demonstration of its light-harvesting performance, we computed the optical absorbance of $PdSeO_3$ monolayer. Note that the electron–hole interactions play a dominant role in the optical properties of 2D materials; however, the ordinary DFT method cannot well treat such exciton effects. Thus, we computed the optical absorbance of $PdSeO_3$ monolayer employing the state-of-the-art *GW*+BSE (Bethe–Salpeter equation) method,[68,69] which considers the electron–electron correlation and electron–hole interactions and thus could well reproduce experimental results. In accordance with our GW computations, the exciton binding energy of $PdSeO_3$ monolayer is 0.6 eV.

As shown in Figure 5, the optical absorbance of $PdSeO_3$ monolayer is anisotropic due to the structure anisotropy. Specifically, in the x direction $PdSeO_3$ has stronger optical absorption in the ultraviolet region than the visible region, while in the y direction the optical absorption in the ultraviolet and visible regions are both very pronounced. Therefore, $PdSeO_3$ monolayer can efficiently harvest sunlight, which would facilitate its utilization as water splitting photocatalyst.

CONCLUSIONS

To summarize, by means of comprehensive DFT computations, we systematically studied the structural, electronic, and optical properties of a novel 2D material, namely $PdSeO_3$ monolayer. In accordance with our computational results, $PdSeO_3$ monolayer has a considerable band gap of 2.84 eV, its VBM and CBM absolutely straddle the redox potentials of water, and the monolayer has strong optical absorbance in both ultraviolet and visible light region. Especially, the photogenerated electrons and holes have adequate driving

http://www.SolidDocuments.com/ Solid PDF Tools

DOI: 10.1021/jacs.8b07855
J. Am. Chem. Soc. 2018, 140, 12256−12262

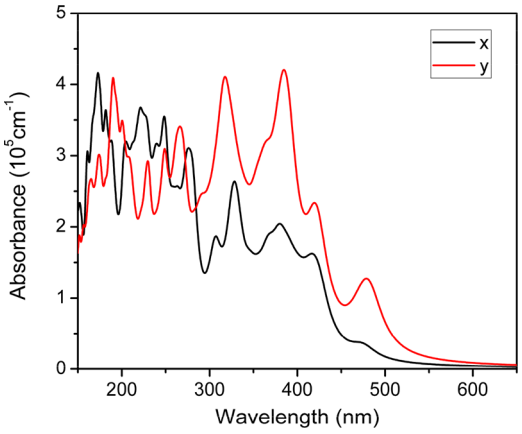

Figure 5. Optical absorbance of $PdSeO_3$ monolayer computed using the GW+BSE method.

forces to render that both water oxidation and hydrogen reduction half reactions proceed spontaneously on the different active sites of the $PdSeO_3$ monolayer. Our results vividly revealed that $PdSeO_3$ monolayer can act as a highly efficient photocatalyst for direct overall water splitting into H_2 and O_2 in a stoichiometric amount of 2:1 without using any sacrificial reagents or cocatalysts. Our findings will help facilitate the exploration and applications of $PdSeO_3$ monolayer and related 2D materials for photocatalysis. Due to the high experimental feasibility, we are rather optimistic that $PdSeO_3$ monolayer could be produced and utilized for photocatalytic water splitting in the very near future.

■ ASSOCIATED CONTENT

Supporting Information

The Supporting Information is available free of charge on the ACS Publications website at DOI: 10.1021/jacs.8b07855.

Structural properties of $PdSeO_3$ bulk and monolayer; snapshots, structure, and energy curves of MD simulations of $PdSeO_3$ monolayer at different temperatures; variation of band edge position and band gap of $PdSeO_3$ nanosheet as a function of thickness; pH dependence of the CBM and VBM of $PdSeO_3$ monolayer in an aqueous electrolyte solution; the free energies of water oxidation intermediates; and ΔG of rate-determining steps of water oxidation and hydrogen reduction reactions for different surface sites of $PdSeO_3$ monolayer (PDF)

■ AUTHOR INFORMATION

Corresponding Authors

*liyafei@njnu.edu.cn

*zhongfangchen@gmail.com

ORCID

Yafei Li: 0000-0003-2587-820X

Zhongfang Chen: 0000-0002-1445-9184

Notes

The authors declare no competing financial interest.

■ ACKNOWLEDGMENTS

Support in China by the Natural Science Foundation of China (nos. 21522305 and 21873050), the NSF of Jiangsu Province of China (BK20150045), and the Priority Academic Program Development of Jiangsu Higher Education Institutions, and in USA by the National Science Foundation-Centers of Research Excellence in Science and Technology (NSF-CREST Center) for Innovation, Research and Education in Environmental Nanotechnology (CIRE2N) (Grant HRD-1736093). The computational resources utilized in this research were provided by Shanghai Supercomputer Center.

■ REFERENCES

(1) Fujishima, A.; Honda, K. *Nature* **1972**, *238*, 37−38.
(2) Walter, M. G.; Warren, E. L.; McKone, J. R.; Boettcher, S. W.; Mi, Q.; Santori, E. A.; Lewis, N. S. *Chem. Rev.* **2010**, *110*, 6446−6473.
(3) Maeda, K.; Domen, K. *J. Phys. Chem. Lett.* **2010**, *1*, 2655−2661.
(4) Qu, Y.; Duan, X. *Chem. Soc. Rev.* **2013**, *42*, 2568−2580.
(5) Chen, S.; Takata, T.; Domen, K. *Nat. Rev. Mater.* **2017**, *2*, 17050.
(6) Tee, S. Y.; Win, K. Y.; Teo, W. S.; Koh, L.-D.; Liu, S.; Teng, C. P.; Han, M.-Y. *Adv. Sci.* **2017**, *4*, 1600337.
(7) Ni, M.; Leung, M. K. H.; Leung, D. Y. C.; Sumathy, K. *Renewable Sustainable Energy Rev.* **2007**, *11*, 401−425.
(8) Cook, T. R.; Dogutan, D. K.; Reece, S. Y.; Surendranath, Y.; Teets, T. S.; Nocera, D. G. *Chem. Rev.* **2010**, *110*, 6474−6502.
(9) Kudo, A.; Miseki, Y. *Chem. Soc. Rev.* **2009**, *38*, 253−278.
(10) Singh, A. K.; Mathew, K.; Zhuang, H. L.; Hennig, R. G. *J. Phys. Chem. Lett.* **2015**, *6*, 1087−1098.
(11) Asai, R.; Morikawa, T.; Ohwaki, T.; Aoki, K.; Taga, Y. *Science* **2001**, *293*, 269−271.
(12) Yanagida, T.; Sakata, Y.; Imamura, H. *Chem. Lett.* **2004**, *33*, 726−727.
(13) Maeda, K.; Takata, T.; Hara, M.; Saito, N.; Inoue, Y.; Kobayashi, H.; Domen, K. *J. Am. Chem. Soc.* **2005**, *127*, 8286−8287.
(14) Tsuji, I.; Kato, H.; Kudo, A. *Angew. Chem., Int. Ed.* **2005**, *44*, 3565−3568.
(15) Ma, G.; Chen, S.; Kuang, Y.; Akiyama, S.; Hisatomi, T.; Nakabayashi, M.; Shibata, N.; Katayama, M.; Minegishi, T.; Domen, K. *J. Phys. Chem. Lett.* **2016**, *7*, 3892−3896.
(16) Maeda, K.; Teramura, K.; Lu, D.; Takata, T.; Saito, N.; Inoue, Y.; Domen, K. *Nature* **2006**, *440*, 295.
(17) Chen, S.; Qi, Y.; Hisatomi, T.; Ding, Q.; Asai, T.; Li, Z.; Ma, S. S. K.; Zhang, F.; Domen, K.; Li, C. *Angew. Chem., Int. Ed.* **2015**, *54*, 8498−8501.
(18) Yang, J.; Wang, D.; Han, H.; Li, C. *Acc. Chem. Res.* **2013**, *46*, 1900−1909.
(19) Novoselov, K. S.; Geim, A. K.; Morozov, S. V.; Jiang, D.; Zhang, Y.; Dubonos, S. V.; Gregorieva, I. V.; Firsov, A. A. *Science* **2004**, *306*, 666−669.
(20) Novoselov, K. S.; Fal'ko, V. I.; Colombo, L.; Gellert, P. R.; Schwab, M. G.; Kim, K. *Nature* **2012**, *490*, 192−200.
(21) Heine, T. *Acc. Chem. Res.* **2015**, *48*, 65−72.
(22) Xu, M. S.; Liang, T.; Shi, M.; Chen, H. *Chem. Rev.* **2013**, *113*, 3766−3798.
(23) Tang, Q.; Zhou, Z.; Chen, Z. F. *Nanoscale* **2013**, *5*, 4541−4583.
(24) Zhang, X.; Zhang, Z.; Wu, D.; Zhang, X.; Zhao, X.; Zhou, Z. *Small Methods* **2018**, *2*, 1700359.
(25) Zhuang, H. L.; Hennig, R. G. *Chem. Mater.* **2013**, *25*, 3232−3238.
(26) Chowdhury, C.; Karmakar, S.; Datta, A. *J. Phys. Chem. C* **2017**, *121*, 7615−7624.
(27) Ma, G.; Chen, S.; Kuang, Y.; Akiyama, S.; Hisatomi, T.; Nakabayashi, M.; Shibata, N.; Katayama, M.; Minegishi, T.; Domen, K. *J. Phys. Chem. Lett.* **2016**, *7*, 3892−3896.
(28) Zhang, X.; Zhao, X.; Wu, D.; Jing, Y.; Zhou, Z. *Adv. Sci.* **2016**, *3*, 1600062.
(29) Ji, Y.; Yang, M.; Dong, H.; Hou, T.; Wang, L.; Li, Y. *Nanoscale* **2017**, *9*, 8608−8615.
(30) Lv, X.; Wei, W.; Sun, Q.; Li, F.; Huang, B.; Dai, Y. *Appl. Catal., B* **2017**, *217*, 275−284.
(31) Jiang, X.; Wang, P.; Zhao, J. *J. Mater. Chem. A* **2015**, *3*, 7750−7758.

Solid PDF Tools
http://www.SolidDocuments.com/

DOI: 10.1021/jacs.8b07855
J. Am. Chem. Soc. 2018, 140, 12256−12262

(32) Lu, S.; Chen, Z. W.; Li, C.; Li, H. H.; Zhao, Y. F.; Gong, Y. Y.; Niu, L. Y.; Liu, X. J.; Wang, T.; Sun, C. Q. *J. Mater. Chem. A* **2016**, *4*, 14827−14838.
(33) Peng, Q.; Xiong, R.; Sa, B.; Zhou, J.; Wen, C.; Wu, B.; Anpo, M.; Sun, Z. *Catal. Sci. Technol.* **2017**, *7*, 2744−2752.
(34) Wang, X.; Maeda, K.; Thomas, A.; Takanabe, K.; Xin, G.; Carlsson, J. M.; Domen, K.; Antonietti, M. *Nat. Mater.* **2009**, *8*, 76−80.
(35) Wang, X.; Maeda, K.; Chen, X.; Takanabe, K.; Domen, K.; Hou, Y.; Fu, X.; Antonietti, M. *J. Am. Chem. Soc.* **2009**, *131*, 1680−1681.
(36) Wang, F.; Shifa, T. A.; He, P.; Cheng, Z.; Chu, J.; Liu, Y.; Wang, Z.; Wang, F.; Wen, Y.; Liang, L.; He, J. *Nano Energy* **2017**, *40*, 673−680.
(37) Shifa, T. A.; Wang, F.; Cheng, Z.; He, P.; Liu, Y.; Jiang, C.; Wang, Z.; He, J. *Adv. Funct. Mater.* **2018**, *28*, 1800548.
(38) Cheng, Z.; Shifa, T. A.; Wang, F.; Gao, Y.; He, J.; Zhang, K.; Jiang, C.; Liu, Q.; He, J. *Adv. Mater.* **2018**, *30*, 1707433.
(39) Schneider, J.; Bahnemann, D. W. *J. Phys. Chem. Lett.* **2013**, *4*, 3479−3483.
(40) Zhang, G.; Lan, Z.-A.; Lin, L.; Lin, S.; Wang, X. *Chem. Sci.* **2016**, *7*, 3062−3066.
(41) Mak, K. F.; Lee, C.; Hone, J.; Shan, J.; Heinz, T. F. *Phys. Rev. Lett.* **2010**, *105*, 136805.
(42) Warner, J. H.; Rümmeli, M. H.; Bachmatiuk, A.; Büchner, B. *ACS Nano* **2010**, *4*, 1299−1304.
(43) Liu, H.; Neal, A. T.; Zhu, Z.; Tománek, D.; Ye, P. D.; Luo, Z.; Xu, X. *ACS Nano* **2014**, *8*, 4033−4041.
(44) Jing, Y.; Ma, Y.; Wang, Y.; Li, Y.; Heine, T. *Chem. - Eur. J.* **2017**, *23*, 13612−13616.
(45) Ling, J.; Albrecht-Schmitt, T. E. *Inorg. Chem.* **2007**, *46*, 5686−5690.
(46) Kresse, G.; Hafner, J. *Phys. Rev. B: Condens. Matter Mat[illegible]hys.* **1993**, *47*, 558−561.
(47) Blöchl, P. E. *Phys. Rev. B: Condens. Matter Mater. Phys.* **1994**, *50*, 17953−17979.
(48) Kresse, G.; Joubert, D. *Phys. Rev. B: Cond[illegible]ter Mater. Phys.* **1999**, *59*, 1758−1775.
(49) Perdew, J. P.; Burke, L.; Ernzerhof, M. *Phys. Rev. Lett.* **1996**, *77*, 3865−3868.
(50) Heyd, J.; Scuseria, G. E.; Ernzerhof, M. *J. Chem. Phys.* **2003**, *118*, 8207−8215.
(51) Grimme, S. *J. Comput. Chem.* **2006**, *27*, 1787−1799.
(52) Baroni, S.; de Gironcoli, S.; Dal Corso, A.; Giannozzi, P. *Rev. Mod. Phys.* **2001**, *73*, 515−562.
(53) Togo, A.; Oba, F.; Tanaka, I. *Phys. Rev. B: Condens. Matter Mater. Phys.* **2008**, *78*, 134106.
(54) Martyna, G. J.; Klein, M. L.; Tuckerman, M. *J. Chem. Phys.* **1992**, *97*, 2635−2643.
(55) Mathew, K.; Sundararaman, R.; Letchworth-Weaver, K.; Arias, T. A.; Hennig, R. G. *J. Chem. Phys.* **2014**, *140*, 084106.
(56) Nørskov, J. K.; Rossmeisl, J.; Logadottir, A.; Lindqvist, L.; Kitchin, J. R.; Bligaard, T.; Jónsson, H. *J. Phys. Chem. B* **2004**, *108*, 17886−17892.
(57) Valdés, Á.; Qu, Z.-W.; Kroes, G. J.; Rossmeisl, J.; Nørskov, J. K. *J. Phys. Chem. C* **2008**, *112*, 9872−9879.
(58) NIST Computational Chemistry Comparison and Benchmark Database, *NIST Standard Reference Database Number 101*, Release 19, April 2018, edited by Russell D. Johnson, III, Available at http://cccbdb.nist.gov/.
(59) Wang, Y.; [illegible]; Chen, Z. *J. Mater. Chem. C* **2015**, *3*, 9603−9608.
(60) Zhu, X.; [illegible]i, F.; Wang, Y.; Qiao, M.; Li, Y. *J. Mater. Chem. C* **2018**, *6*, 4494−4500.
(61) Zacharia, R.; Ulbricht, H.; Hertel, T. *Phys. Rev. B: Condens. Matter Mater. Phys.* **2004**, *69*, 155406.
(62) Molina-Sánchez, A.; Wirtz, L. *Phys. Rev. B: Condens. Matter Mater. Phys.* **2011**, *84*, 155413.
(63) Cahangirov, S.; Topsakal, M.; Akturk, E.; Sahin, H.; Ciraci, S. *Phys. Rev. Lett.* **2009**, *102*, 236804.
(64) Xu, Y.; Schoonen, M. A. A. *Am. Mineral.* **2000**, *85*, 543−556.
(65) Chen, S.; Wang, L.-S. *Chem. Mater.* **2012**, *24*, 3659−3666.
(66) Zhang, Y.; Antonietti, M. *Chem. - Asian J.* **2010**, *5*, 1307−1311.
(67) Wirth, J.; Neumann, R.; Antonietti, M.; Saalfrank, P. *Phys. Chem. Chem. Phys.* **2014**, *16*, 15917−15926.
(68) Rohlfing, M.; Louie, S. G. *Phys. Rev. B: Condens. Matter Mater. Phys.* **2000**, *62*, 4927−4944.
(69) Onida, G.; Reining, L.; Rubio, A. *Rev. Mod. Phys.* **2002**, *74*, 601−659.

Solid PDF Tools http://www.SolidDocuments.com/

DOI: 10.1021/jacs.8b07855
J. Am. Chem. Soc. 2018, 140, 12256−12262